Use of 2D Nanoplatelets to Improve The Sensitivity in Hybrid Photodetector For Indirect X-Ray Imaging

Jehoon Lee
Dankook University
Kyunghan Yoo
Dankook University
Hailiang Liu
Dankook University
Jungwon Kang (jkang@dankook.ac.kr)
Dankook University

Research Article

Keywords: Polymer, Nanoplatelets, X-ray Detector, Hybrid Active Layer

Posted Date: October 26th, 2021

DOI: https://doi.org/10.21203/rs.3.rs-988889/v1

Abstract

In this paper, we attempted to improve the detection sensitivity of an indirect X-ray detector through using a hybrid active layer composed of a poly [N-90-heptadecanyl–2,7-carbazole-alt-5,5-(40,70-di-2-thienyl-20,10,30-benzothiadiazole)] (PCDTBT) organic semiconductor and cadmium selenide nanoplatelets (CdSe NPLs) colloidal inorganic semiconductors. First, different blending ratio in the active layer (i.e., 2:1, 1:1, 1:2 and 1:3) of PCDTBT:CdSe NPL were examined, a sensitivity of 0.057 mA/Gy•cm^2 was achieved using a 1:1 ratio due to the low series resistance (R_S) and defect density in this configuration. Then, the oleic acid (OA) that was initially applied in the CdSe NPL surface was replaced with pyridine ligands, this was done because the pyridine ligand is a short-chain ligand that can help charge transfer by reducing the distance between NPLs in the active layer. In addition, an experiment was conducted to determine the optimal ligand exchange time. A detector with an PCDTBT:CdSe NPL active layer fabricated using pyridine ligand exchange achieved a sensitivity of 0.14 mA/Gy•cm^2 after an exchange time of 12 hours, this is an improvement of 155% compared to the detector using a PCDTBT:CdSe NPL with the original OA ligands. Lastly, the optimal thickness for the PCDTBT:CdSe NPL active layer was investigated. The highest mobility of 7.60 cm^2/V•s was recorded after fabricating the layer using spin-coating at 1900 rpm, the highest sensitivity of 0.20 mA/Gy•cm^2 was also achieved under these conditions. Compared to the initial state of the detector, our modifications improved the sensitivity of the PCDTBT:CdSe NPL detector by 255%.

Introduction

Nanocrystals (NCs) have attracted attention as crystallines with a nanometer range (in at least one dimension) due to the advantages this provides in terms of high carrier mobility [1, 2] and excellent optical properties such as efficient photon absorption [3]. In addition, when the NCs are smaller than the exciton's Bohr radius, the optical and electrical properties are affected by the shapes and size of the NCs because which are determined by the quantum confinement effect. Therefore, it becomes possible to adjust the bandgap by changing the size of the NCs. These NCs can be synthesized with semiconductor material compositions such as those in groups II-VI (CdSe, CdS, CdTe, ZnS), IV-VI (PbS, PbSe, PbTe), and III-V (InP, GaAs). Among these materials, cadmium-based NCs have been extensively studied as an emitter or as a light-harvesting material [4–6] because their bandgap is in the visible light region. Cadmium-based NCs have several shapes, such as dots [7, 8], wires [9], tetrapods [10], and plates [11, 12]. The plate-shaped NC is a two-dimension (2D) anisotropic structure in which electron-hole pairs are strongly confined according to thickness, these 2D NCs can be obtained by controlling their thickness during fabrication with atomic-level precision. 2D NCs prevent Auger recombination due to their low-energy disordered properties [13, 14], they also generate additional excitons due to the multi-exciton formation make possible. This has the additional advantages of low carrier loss [15] with only small Stokes shifts helping optical energy and charge transfer [16].

The 2D NCs can be mixed with organic semiconductor materials to form hybrid semiconductors, integrating the advantages of each other in one place. The NCs are physically and chemically stable [17] compared to the organic semiconductors, this can help overcome the photo-induced degradation of the organic semiconductors. The NCs can transfer fast photo-induced charge carriers to the organic semiconductors because the transfer rate is faster than the recombination mechanism. Therefore, the charge is able to efficiently transfer between the organic materials as donors to the NCs as acceptors. Furthermore, this combination means optical energy transfers such as the Förster resonance energy transfer (FRET) [18, 19] and forming additional multi-excitons becomes possible [20]. The organic/NCs hybrid semiconductors are suitable for large scale, easy fabrication processing, and physically flexible devices [21] because of their solution processability. Therefore, they can be used as active materials in a variety of applications such as in light-emitting diodes (LEDs) [22], photodetectors [23], biomedical labelling [24], and radiation detectors [25]. Among these, in the field of radiation detectors, hybrid active layer research with these organic/NCs hybrid semiconductors is underway with the goal of improving detection sensitivity [26, 27].

In this paper, we conducted experiments to improve the detection sensitivity of an indirect X-ray detector with a hybrid active layer, this layer was synthesized with 2D cadmium-based NPLs combined with an organic semiconductor. The hybrid active layer was composed of a p-type organic semiconductor, poly [N-90-heptadecanyl–2,7-carbazole-alt-5,5-(40,70-di-2- thienyl-20,10,30-benzothiadiazole)] (PCDTBT), as the donor and n-type inorganic NCs, cadmium selenide nanoplatelets (CdSe NPLs), as the acceptor. In terms of molecular structure, PCDTBT was selected because it has an alkyl chain that promotes covalent inter-molecule bonding and it helps form a percolation path when mixed with an acceptor, leading to improved detector performance [28]. Experiments were conducted to investigate the effects of the blending ratio, ligand exchange on the CdSe NPL surface and spin-coating conditions on the performance of the hybrid active layer. Figure 1 (a) shows the structure of a detector with this PCDTBT:CdSe NPL hybrid active layer, which forms a bulk heterojunction (BHJ). The detector, which has no scintillator, works as a photodetector, we evaluated its series resistance (R_S), mobility, and defect density, which was extracted from the current density-voltage (J-V) curve, while using an artificial solar simulator. The corresponding energy-band diagram of the proposed detector structure and materials is depicted in Figure 1 (b). Conventionally, detectors with a CsI(Tl) scintillator are used for X-ray imaging measurements [29, 30] due to their high detection efficiency and a long lifetime. The CsI(Tl) scintillator converts X-ray photons into visible-light photons with a peak of 560 nm wavelength for indirect-type X-ray detector characterization. The converted visible-light photons are then absorbed by a donor material to form excitons, which separate into electrons and holes at the donor/acceptor interface, with each being collected by the appropriate electrode according to the energy band. Through this collected charge, evaluates the radiation detector characteristics such as collected current density (CCD), dark current density (DCD), sensitivity, and linearity.

Experimental Detail

1.1. Materials

Sodium myristrate (99.9%), cadmium nitrate (99.997%), selenium powder (100 mesh, 99.99%), cadmium acetate dihydrate (reagent grade, 98%), methanol (HPLC grade, 99.9%), 1-octadecene (ODE, 90%), hexane (HPLC grade, 95.0%), ethyl alcohol (200 proof, HPLC grade), DMF (HPLC grade, 99.9%), and chlorobenzene (HPLC grade, 99.9%).

1.2 CdSe Nanoplatelets (NPLs) synthesis

Precursors such as cadmium myristate ($Cd(Myr)_2$) and selenium ODE (SeODE) were prepared for CdSe NPLs synthesis (see Electronic Supplementary Materials for details on the synthesis processes).

1.2.1 Synthesis of the 4 monolayers (MLs) thick CdSe NPLs

Using a 50 mL three-neck flask, 100 mg (0.173 mmol) of $Cd(Myr)_2$, 16 mg (0.2 mmol) of selenium powder and 10 mL of ODE were degassed under vacuum at 110℃ over 20 min. After that, the mixture was heated to 140℃ and maintained for 20 min so the precursors could dissolve. The temperature was then increased to 240℃, as the temperature of the mixture increased 61.3 mg (0.23 mmol) of cadmium acetate dihydrate ($Cd(OAc)_2•2H_2O$) was added quickly between 180 ~ 210℃ after the solution had turned yellow in color. After the solution was maintained at 240℃ for an additional 8 min before the flask was removed from the heating mantle and the mixture was allowed to cool down. At 160℃, 1.33 ml of oleic acid (OA) was injected using a syringe. When the resulting solution reached room temperature, hexane and ethyl alcohol were added in a 3:1 ratio and the mixture centrifuged at 6000 rpm for 10 min to obtain 4 ML-thick CdSe NPLs.

1.2.2 Synthesis of the 5 monolayers (MLs) thick CdSe NPLs

Using a 50 mL three-neck flask, 113 mg (0.2 mmol) of $Cd(Myr)_2$, 8 mg (0.1 mmol) of selenium powder and 10 mL of ODE were degassed under vacuum at 110℃ over 20 min. After that, the mixture was heated to 140℃ where it was maintained for 20 min to dissolve the precursors. The temperature was then increased to 240℃, while the temperature of the mixture was increasing 125 mg (0.47 mmol) of $Cd(OAc)_2•2H_2O$ was added quickly between 180 ~ 210℃ after the solution had turned yellow in color. After being maintained at 240℃ for 10 min, SeODE 1 mL was added. The solution was then maintained at 240℃ for an additional 5 min before the flask was removed from the heating mantle allowing the mixture to cool. At 160℃, 0.67 mL of OA was injected using a syringe. For selective precipitation, hexane and ethyl alcohol were added to the resulting solution at a 3:1 ratio. Finally, the solution was centrifuged at 6000 rpm for 10 min to obtain 5 ML-thick CdSe NPLs.

Figure 2 shows the optical properties, such as absorbance and emission spectrum, of the synthesized cadmium selenide nanoplatelets (CdSe NPLs), with either 4 and 5 monolayers (MLs), here the results are compared with a CsI(Tl) scintillator emission spectrum. The 4 and 5 ML-thick NPLs were found to be 1.8 nm and 2.1 nm thick, respectively, with emission peak of 513 and 551 nm wavelengths. Since the

thicknesses of both the synthesized CdSe NPLs are smaller than the bore radius (5.4 nm) of CdSe, quantum confinement effects can be seen but only in the thickness direction. This gives the CdSe NPLs' emissions narrow full-width at half-maximum (FWHM) values of 8 and 11 nm, respectively, while experiencing small Stokes shifts of less than 1 nm. The synthesized CdSe NPLs show two peaks in their absorbance wavelengths, these appear according to the effective mass (m*) of the hetero-material. If the effective mass is low, defined as a light-hole (LH), whereas if the effective mass is high, defined as a heavy-hole (HH), this is shown by the valence band in the e-k diagram. The HH has low energy because its effective mass is relatively high and low mobility then LH, the charge carrier characteristics appear according to HH position. Therefore, we can conclude emissions from the nanoplatelets come from a HH position [31]. In order to use CdSe NPLs with an indirect X-ray detector in its hybrid active layer, the 5 ML-thick CdSe NPL with good absorbance matching with CsI(Tl) scintillator emission spectrum was selected and evaluated.

Figure 3 shows a transmission electron microscopy (TEM) image and the X-ray diffraction (XRD) pattern of the synthesized 5 ML-thick CdSe NPLs. In the TEM image, we can see the CdSe NPLs are in the form of two-dimensional nanoplates, 35.2 and 11.0 nm in length and width, respectively, with a thickness of about 2 nm. In semiconductor compounds, cubic (zinc-blend structures) and hexagonal (wurtzite structures) are common crystal structures. The zinc-blend structure is high density and thermodynamically preferable to the wurtzite structure [32]. In addition, zinc-blend structure exhibits very narrow excitonic features without inhomogeneous broadening [33]. The XRD pattern shows that the CdSe NPLs have a zinc-blend crystalline structure. The experimental diffraction maximum of the CdSe NPLs were found to be at 2θ = 25.3, 41.5, 49.5 and 60.1°, which closely coincide with the respective (111), (220), (311), and (400) reflections from a cubic (zinc-blended) crystal structure. Looking at the XRD data in Figure 5 (b), we can confirm that a zinc-blend structure CdSe NPLs were synthesized.

1.3 Detector fabrication

Figure 4 shows the fabrication process of the photodetector with a PCDTBT:CdSe NPL hybrid active layer. First the ITO-patterned glass substrate was cleaned with acetone using an ultrasonic bath for 5 min, this was then repeated with methanol then finally isopropyl alcohol (IPA). The cleaned substrate was baked in a vacuum oven at 100℃ for 10 min before being treated for 15 min using UV light to give a hydrophilic surface to the substrate. For the hole transport layer (HTL) coating, poly(3,4-ethylenedioxythiophene):poly(styrenesulfonate) (PEDOT:PSS) (CLEVIOS Al 4083) blended with dimethylformamide (DMF) 50 wt% was spin-coated onto the cleaned substrate at 3000 rpm for 30 seconds using a spin-coater (Dong Ah ACE-200). After that, the sample was baked at 160℃ for 30 min to vaporize any residual DMF solvent. The poly[N-90-heptadecanyl–2,7-carbazole-alt-5,5-(40,70-di-2-thienyl-20,10,30-benzothiadiazole)] (PCDTBT) and cadmium selenide nanoplatelets (CdSe NPLs) were dissolved in chlorobenzene, the solution was then stirred for 3 h at 90℃. Next, the PCDTBT:CdSe NPL solution was spin-coated onto the HTL at 1300 rpm over 30 sec. Then, this active layer was baked at 150℃ for 10 min, before a 120 nm-thick aluminum (Al) cathode was deposited using a thermal evaporator under a pressure

of 10^{-5} torr. Finally, an encapsulation process was carried out to prevent any penetration from moisture or oxygen.

1.4 Method used to extract experimental parameters

Evaluations of the fabricated detector's characteristics were carried out in two ways: with and without a CsI(Tl) scintillator. First, the detector without the CsI(Tl) scintillator (Hamamatsu J13113) was evaluated as a photodetector for measuring the series resistance (R_S) and J-V curve under the light of an artificial solar simulator using an AM 1.5G filtering Xe lamp (San Ei Electronics XES-40S2-CE). R_S was defined as the inverse of the slope of the J-V curve for the voltage range where no current was flowing while the bias voltage being applied to the detector was increased. The distance between the solar simulator and detector was kept at 25 cm while under light exposure of 100 mW/cm^2. The generated charge was collected by applying a bias from -1.0 to +2.0 V. Next, the detector was coupled with the CsI(Tl) scintillator to evaluate its characteristics as an X-ray detector in terms of collected current density (CCD), dark current density (DCD), and sensitivity. The experimental set-up consisted of an X-ray generator (AJEX 2000H) and a sourcemeter (Keithley 2400) for measuring the generated charge during on and off X-ray irradiation, as shown in Figure 5.

The X-ray generator was operated with a tube voltage of 80 kV_p, a tube current of 63 mA•s, and an exposure time of 1.57 seconds. The distance between the X-ray generator and the detector was fixed at 30 cm. The exposed X-ray dose was measured using an ion chamber (Capintec CII50) at the same distance from the generator as the detector. The exposure dose was converted to an absorbed dose, which was measured using the ion chamber. Under the conditions outlined above, the absorbed dose was found to be 3.34 mGy. The applied voltage on the detector was set in the range of -0.2 to -2.0 V while obtaining the CCD, DCD, and sensitivity according to the respective following equations:

$$\mathrm{CCD} = \frac{Collected\ \ Current\ \ during\ \ X-ray\ \ ON}{\mathrm{Exposed\ \ Detection\ \ Area}} \quad (1)$$

$$\mathrm{DCD} = \frac{Collected\ \ Current\ \ during\ \ X-ray\ \ OFF}{\mathrm{Exposed\ \ Detection\ \ Area}} \quad (2)$$

$$\mathrm{Sensitivity} = \frac{CCD - DCD}{\mathrm{Absorbed\ \ Dose} \times \mathrm{Exposed\ \ Area}} \quad (3)$$

Results And Discussion

2.1. Experiments regarding the PCDTBT:CdSe NPL blending ratio

The detector was evaluated while using PCDTBT:CdSe NPL hybrid active layers with various blending ratios. The amount of PCDTBT used was fixed at 5 mg while the blending ratio was adjusted by adding

suitable amounts of CdSe NPLs to give ratios of 2:1, 1:1, 1:2, and 1:3. This was done to confirm optimal PCDTBT:CdSe NPL blending ratio to use in the active layer. First, the absorbance of the film state active layer and the CsI(Tl) scintillator emission spectrums according to the PCDTBT:CdSe NPL blending ratio are shown in Figure 6 (a). The absorption of the PCDTBT:CdSe NPL film tends to increase as the amount of CdSe NPLs increases. Figure 6 (b) shows the obtained X-ray detector parameters such as the collected current density (CCD) and sensitivity according to the PCDTBT:CdSe NPL blending ratio. Unlike the trend noticed with the absorbance, the highest sensitivity of 0.0566 mA/Gy•cm^2 was found with a 1:1 blending ratio. When the ratio of PCDTBT increases in the hybrid blend, the generated charge transfer decrease due to decreases in the amount of CdSe NPLs that can act as acceptors. In contrast, if the CdSe NPLs ratio becomes too high, trap sites that cause generated charge recombination are created. As such, the 1:1 blending ratio was found to be the optimum PCDTBT:CdSe NPL blending ratio.

To understand the differing trends between the detector's absorbance and X-ray parameters, a comparison experiment was conducted that looked at defect density and R_S. Figure 7 (a) shows a J-V curve recorded under dark conditions that can be used to calculate trap density, this done while representing the X and Y axes on a log scale and using the following defect density equation:

$$N_{defects}\ (Defect\ \ density) = \frac{2\varepsilon_r \cdot \varepsilon_0 \cdot V_{TFL}}{q \cdot L^2} \quad (4)$$

where $N_{defects}$ is the defect density, ε_r is the complex dielectric constant of the PCDTBT:CdSe NPL, ε_0 is the permittivity of free space (8.854 X 10^{-4} F/m), q is the elementary charge (1.602 X 10^{-19} C), and L is the thickness of the PCDTBT:CdSe NPL film, which was measured using a surface profiler (KLA-Tencor Alpha-step AS-500). Also, V_{TFL} is defined as the trap-filled limit voltage, this represents the voltage at the point where the trap-limited space-charge limit current (SCLC) and the trap-filled limit region overlap on the log scale J-V curve recorded under dark conditions. The extracted defect density and R_S are shown in figure 7 (b). Since the defect density gives an indication of how many trap sites that cause charge recombination there are in the PCDTBT:CdSe NPL active layer, any reduction in defect density improves the stability of the detector [34]. When comparing the defect density according to the PCDTBT:CdSe NPL blending ratio, it was most significantly reduced at a ratio of 1:1 with a trap density of 1.02 x 10^{17} cm^{-3}. In addition, R_S, which affects the current transfer of the detector, was also the lowest at a 1:1 blending ratio (R_S = 81 kΩ). Therefore, the hybrid PCDTBT:CdSe NPL blending ratio of 1:1 gives the lowest defect density and R_S making it the optimal blending ratio.

2.2 Experiments regarding CdSe NPLs ligand exchange

To ensure the best charge transport conditions in the active layer, the optimal PCDTBT:CdSe NPL blending ratio of 1:1 was fixed for all further experiments. In our first experiment the oleic acid (OA) ligand on the CdSe NPL surface was exchanged with pyridine ligand. The OA ligand is a kind of long-chain ligand that helps with dispersion in a solution, but has the disadvantage of interfering with charge transport between NPL particles [35]. In contrast, as short-chain ligands such as pyridine, 3-

mecaptopropionic acid (MPA), and 1,2-ethylenedithiol (EDT) shorten the distance between CdSe NPL particles, they thereby increase interactions with organic material and improve charge transport properties [36, 37]. Among these short-chain ligands, we chose to apply pyridine ligand in our experiments due to its good electrical conductivity. However, if the proportion of pyridine in the NPL surface is increased too much, the distance between the NPL particles becomes too small leading to aggregation. Considering these characteristics, experiments were performed to change the ratio of ligands by adjusting the ligand exchange time, thermogravimetric analysis (TGA) measurements were then performed to confirm the appropriate ratio of ligands. To proceed with the ligand exchange experiments, CdSe NPLs with OA ligand dispersed in toluene was mixed with pyridine in a 5:2 ratio, before being heated to 30℃ where it was maintained overnight. After that, the mixed solution was added to methanol in a 1:1 ratio and centrifugation was performed. At this point various ligand exchange times were used to produce different ligand ratios: 0, 6, 12, 18 and 24 hours. TGA measurements were then performed on the CdSe NPLs with OA ligand as well as on the CdSe NPLs after pyridine ligand exchange, the results of two conditions (0 and 12 hours) for comparison are shown in figure 8 (a).

In the CdSe NPLs with OA ligand sample, weight loss of the OA ligands starts around the boiling point at 286℃ and continues until 500℃. The total weight loss was equal to 26.36% of the starting weight, indicating the CdSe NPLs were covered by only OA ligands. The TGA curve for the CdSe NPLs with exchanged pyridine ligands has more than one step. The weight loss was 7.22% from the pyridine boiling point at 115℃ to the intermediate plateau temperature at 362.63℃ while the total weight loss below 362.63℃ was 19.53%. We estimated the fraction of CdSe NPL surface sites covered by pyridine and OA ligands [38]. The surface coverage of pyridine ligands was calculated to be 50.74% while the surface coverage of OA ligands was 38.43% after the12-hours ligand exchange time. All surface coverages according to the pyridine ligand exchange time are shown in Figure 8 (b).

The TGA measurements determined the OA to pyridine ligand coverage ratio according to the ligand exchange time and evaluated the detector with PCDTBT:CdSe NPL covered OA and pyridine ligand. Figure 9 (a) shows an active layer AFM image of the film's state according to the pyridine ligand exchange time. The average surface roughness (R_q) increases rapidly as the pyridine ligand exchange time increases from the 6-hour exchange time and continues to increase over time since the distance between the particles becomes closer and closer while agglomeration occurs. As a photo and X-ray detector, R_S, defect density, CCD, and sensitivity were evaluated and shown in Figure 9 (b). The R_S trend of the detector changed because R_S is affected by the defects present in the active layer. Therefore, the defect density according to the ligand exchange time was calculated and compared to the R_S trend. As the ligand exchange time increased from 0-, 6-, 12-, 18-, and 24-hour, the R_S recorded were 81.4, 74.8, 32.6, 42.8, and 51.4 kΩ, while the defect densities recorded were 10.2, 9.96, 9.62, 9.71, and 9.76 x 10^{16} cm^{-3}, respectively. The defect density and R_S trends were similar with the lowest R_S and defect density coming after the 12-hour ligand exchange time. Since the electrical properties were also improved under the same conditions for the best R_S and defect density, the CCD and sensitivity were also highest at 0.62935 μA/cm^2 and 0.1444 mA/Gy•cm^2 after the 12-hour ligand exchange time. As such, the 12-hour ligand

exchange time was identified as optimal and the spin-coating experiments were conducted using active layers that were fabricated using a 12-hour ligand exchange time.

2.3 Experiments regarding the spin-coating conditions of the PCDTBT:CdSe NPL hybrid active layer

Finally, experiments were conducted to find the optimal spin-coating conditions to use when fabricating the PCDTBT:CdSe NPL hybrid active layer. The thickness of the active layer was adjusted by setting the spin rate of the spin-coater to one of 1000, 1300, 1600, 1900, or 2200 rpm, the previous active layers were formed using a 1300 rpm spin rate. The thickness of the active layers were measured using a surface profiler (KLA-Tencor Alpha-step AS-500). The carrier mobility of the detector was also calculated to determine the charge transport characteristics according to the spin-coating condition of the active layers. The carrier mobility was calculated using the space charge limited current (SCLC) model, with a slope of 2 in the log scale J-V curves under dark conditions, and using the following Mott-Gurney equation [39, 40]:

$$\text{Carrier mobility } (\mu) = \frac{8}{9} \cdot J \cdot \frac{L^3}{V_a{}^2 \cdot \varepsilon_0 \cdot \varepsilon_r} \quad (5)$$

where, J is the current density, L is the thickness of the PCDTBT:CdSe NPL active layer and V_a is the applied voltage in the SCLC region, ε_0 is the free-space permittivity constant of a vacuum (8.85 x 10^{-12} F/m) and εr is the relative permittivity of the applied material. The relative permittivity of the blended PCDTBT:CdSe NPL material was determined using the permittivity equation for blended materials [41] where the relative permittivity was calculated according to the spin rate. Figure 10 (a) shows the log-scale X, Y graph used to extract the mobility and defect densities at spin rates of 1300 and 1900 rpm. The defect density calculation is presented in section 2.1, while the mobility, defect density, thickness and detection sensitivity according to the spin rate are shown in Figure 10 (b). As the spin rate increases, the thickness tends to decrease from 90, 88, 84, 81, to 76 nm, respectively. The measured thickness were then applied to the mobility and defect density calculations, the results showed mobility tends to increase up to 1900 rpm before then decreasing as the rpm is further increased with respective calculated values of 3.92, 4.39, 5.83, 7.60, and 6.83 x 10^{-6} $cm^2/V•s$. Conversely, the defect density decreases up to 1900 rpm and then increases after with respective calculated values of 10.89, 9.64, 9.62, 9.31, and 9.40 x 10^{17} cm^{-3}. Comparing the 1300 rpm pristine spin rate used with the 1900-rpm rate, the mobility improved by 73.12% while the defect density was reduced by 3.42%. These results suggest that adjusting the spin-coating condition of the PCDTBT:CdSe NPL hybrid active layer can significantly improve the charge transport, which makes using the optimal thickness important to realizing a high-performance detector. In addition, the PCDTBT:CdSe NPL hybrid detector was found to also achieve the highest sensitivity of 0.20 $mA/Gy•cm^2$ at a spin rate of 1900 rpm, giving a 39.13% improvement compared to the pristine spin rate of 1300 rpm.

In order to confirm the performance of an X-ray detector with a PCDTBT:CdSe NPL hybrid active layer, the linearity of the sensitivity was measured according to the applied voltage and absorbed dose during X-ray

irradiation. The voltage applied to the PCDTBT:CdSe NPL hybrid detector was set in the range from -0.2 to -2.0 V, as shown in Figure 11 (a). It was found the CCD and sensitivity of the detector with the PCDTBT:CdSe NPL hybrid active layer tends to saturate at -1.4 V. The results of experiments conducted to look at the CCD-DCD as the absorbed dose of radiation was changed in the range 0.55 ~ 5.46 mGy are shown in Figure 11 (b), these were performed using an applied voltage of -1.4 V. As shown in Equation (3), the two values (CCD and DCD) should have a linear relationship, the coefficient of determination (R^2) of the linear relationship for our detector was 0.994, while the slope of the fitted linear line was similar to the measured sensitivity of 0.20 mA/Gy•cm^2.

Conclusions

In this paper, we conducted experiments with the goal of improve the detection sensitivity of an indirect X-ray detector with a hybrid active layer composed of poly[N-90-heptadecanyl–2,7-carbazole-alt-5,5-(40,70-di-2-thienyl-20,10,30-benzothiadiazole)] (PCDTBT) organic semiconductor and cadmium selenide nanoplatelet (CdSe NPL) inorganic semiconductors. The NPLs have offer improved performance in terms of optical properties, chemical stability and physical characteristics compared to quantum dots (QDs) and nanowires (NWs). The CdSe NPLs were synthesized to be either 4 or 5 monolayers (MLs) thick, while zinc-blend structures were confirmed through TEM and XRD measurements. Among the two-types of CdSe NPL fabricated, the 5-ML thick NPLs were used due to the good match they provided between the CsI(Tl) scintillator emission spectrum position and the NPL's absorbance spectrum peak. To improve the detection sensitivity of a detector with the PCDTBT:CdSe NPL hybrid active layer, an experiment was performed to find the optimal PCDTBT:CdSe NPL blending ratio in the range of ratios from 2:1 to 1:3, film absorbance was also measured according the blending ratio. As the NPL contents were increased in the active layer, the film absorbance also increased as the NPLs have a high absorption coefficient. The CCD and sensitivity of detectors with active layers of various ratios under the same conditions was measured under X-ray irradiation. As the blending ratio became less than 2:1, the absorbance reduced and while the blending ratio was increased from 1:3, the amount of NPLs was increased, resulting in charge traps forming within the active layer, leading to reduced charge transport. Thereafter, a surface ligand exchange experiment was conducted to improve the sensitivity of the detector while using the optimal PCDTBT:CdSe NPL blending ratio of 1:1 in the active layer. The first applied ligand, OA, was exchanged with pyridine ligands, a short-chain ligand in order to help charge transfer by reducing the distance between NPLs in the PCDTBT:CdSe NPL active layer. The ligand exchange experiment was performed ligand exchange times ranging from 0 (no ligand exchange) to 24 hours. It was found that after a 12-hour ligand exchange period, the pyridine ligand covered for 50.74% while the OA ligand covered for 38.43% of the CdSe NPL surface, resulting in a total surface ligand exchange of 89.17%. If the ligands were exchanged for more than 12-hour, the pyridine ligand exchange continued, and the distance between the NPLs was further reduced, resulting in aggregation and the detector properties deteriorating. It was found that the sensitivity of the detector with a PCDTBT:CdSe NPL active layer after a ligand exchange time of 12 hour was improved by 155% compared to a detector with a PCDTBT:CdSe NPL active layer that did not undergo ligand exchange (i.e., 0 hours). To further improve the detection sensitivity, an experiments

were conducted where the thickness of the active layer was adjusted by changing the spin rate in the range from 1000 to 2100 rpm. The previous optimization experiments were carried out using a 1300 rpm spin rate that gave an active layer thickness of 88 nm. The thickness decreased with increasing spin rate, the detector achieved a highest sensitivity of 0.20 mA/Gy•cm^2 after using a spin rate 1900 rpm (producing an 81 nm-thick layer). Compared to the pristine detector, the sensitivity of the detector with a PCDTBT:CdSe NPL fabricated using a 1900-rpm spin rate was improved by 255%. In order to confirm the performance of the detector with a PCDTBT:CdSe NPL hybrid active layer, the linearity of sensitivity was measured according to applied voltage and absorbed dose during X-ray irradiation. Experiments looking at CCD-DCD according to changes in the absorbed dose of radiation in the range from 0.55 ~ 5.46 mGy were conducted. The coefficient of determination (R^2) of the linear relationship was 0.994, while the slope of the fitted linear line was similar to the measured sensitivity of 0.20 mA/Gy•cm^2.

Declarations

Acknowledgements

This research was supported by National R&D Program through the National Research Foundation of Korea(NRF) funded by Ministry of Science and ICT(2021M3H2A1038042).

References

1. Nguyen, L. N., Chang, W. H., Chen, C. D. & Lan, Y. W. Superior phototransistors based on a single ZnO nanoparticle with high mobility and ultrafast response time. *Nanoscale Horiz*, **5**, 82–88 (2020).
2. Jang, Y. *et al.* High field-effect mobility pentacene thin-film transistors with nanoparticle polymer composite/polymer bilayer insulators. *Appl. Phys. Lett*, **94**, 183301 (2009).
3. Zhu, B. H. *et al.* Size confinement and origins of two-photon absorption and refraction in CdSe quantum dots. *Opt. Express*, **27**, 1777–1785 (2019).
4. Hegazy, M. A. & El-Hameed, A. M. A. Characterization of CdSe-nanocrystals used in semiconductors for aerospace applications: Production and optical properties. *NRIAG J. Astron. Geophys*, **3**, 82–87 (2014).
5. Huang, X. P., Parashar, V. K. & Gijs, M. A. M. Spontaneous Formation of CdSe Photoluminescent Nanotubes with Visible-Light Photocatalytic Performance, ACS Cent. *Sci*, **5**, 1017–1023 (2019).
6. Salem, A. *et al.* Synthesis and characterization of CdSe nanoparticles via thermal treatment technique. *Results Phys*, **7**, 1556–1562 (2017).
7. Ratnesh, R. K. & Mahata, M. S. Controlled synthesis and optical properties of tunable CdSe quantum dots and effect of pH. *AIP Adv*, **5**, 097114 (2015).
8. Hu, M. Z. & Zhu, T. Semiconductor Nanocrystal Quantum Dot Synthesis Approaches Towards Large-Scale Industrial Production for Energy Applications. *Nanoscale Res. Lett*, **10**, 469 (2015).

9. Yu, H. *et al.* Cadmium selenide quantum wires and the transition from 3D to 2D confinement. *J. Am. Chem. Soc*, **125**, 16168–16169 (2003).
10. Heo, H. *et al.* Assemblies of Colloidal CdSe Tetrapod Nanocrystals with Lengthy Arms for Flexible Thin-Film Transistors. *Nano Lett*, **17**, 2433–2439 (2017).
11. Singh, S. *et al.* Colloidal CdSe Nanoplatelets, A Model for Surface Chemistry/Optoelectronic Property Relations in Semiconductor Nanocrystals. *J. Am. Chem. Soc*, **140**, 13292–13300 (2018).
12. Bouet, C. *et al.* Two-Dimensional Growth of CdSe Nanocrystals, from Nanoplatelets to Nanosheets. *Chem. Mater*, **25**, 639–645 (2013).
13. Li, Q. Y. *et al.* Size-Independent Exciton Localization Efficiency in Colloidal CdSe/CdS Core/Crown Nanosheet Type-I Heterostructures. *ACS Nano*, **10**, 3843–3851 (2016).
14. Philbin, J. P. *et al.* Area and thickness dependence of Auger recombination in nanoplatelets. *J. Chem. Phys*, **153**, 054104 (2020).
15. Rowland, C. E. *et al.* Picoscend energy transfer and multiexciton transfer outpaces Auger recombination in binary CdSe nanoplatelet solids. *Nat. Mater*, **14**, 484–489 (2015).
16. Yu, J. H. & Chen, R. Optical properties and applications of two-dimensional CdSe nanoplatelets, InfoMat 2020, 2, 905-927.
17. Phan, H. T. & Haes, A. J. What Does Nanoparticles Stability Mean? *J. Phys. Chem. C*, **123**, 16495–16507 (2019).
18. Lee, J., Liu, H. & Kang, J. A Study on an Organic Semiconductor-Based Indirect X-ray Detector with Cd-Free QDs for Sensitivit Improvement, Sensors 2020, 20, 6562.
19. Han, Y. W., Jeon, S. J., Choi, J. Y., Kim, J. H. & Moon, D. K. Highly efficient Ternert Solar Cells of 10.2% with Core/Shell Quantum Dots via FRET Effect. *Sol. RRL*, **2**, 1800077 (2018).
20. Steiner, A. M., Lissel, F., Fery, A., Lauth, J. & Scheele, M. Prospects of Coupled Organic-Inorganic Nanostructures for Charge and Energy Transfer Applications. *Angew. Chem. Int. Ed*, **60**, 1152–1175 (2020).
21. Lee, J. & Kang, J. Characteristics of a Flexible Radiation Detector Fabricated with Non-Fullerene Acceptor for an Indirect-type X-ray Imaging. *J. Instrum*, **14**, C03008 (2019).
22. Zhang, F. J. *et al.* Super color purity quantum dot light-emitting diodes fabricated by using CdSe/CdS nanoplatelets. *Nanoscale*, **8**, 12182–12188 (2016).
23. Luo, S. P., Kazes, M., Lin, H. & Oron, D. Strain-Induced Type II Band Alignment Control in cdSe Nanoplatelet/ZnS-Sensitized Solar Cells. *J. Phys. Chem. C*, **121**, 11136–11143 (2017).
24. Bolotsky, A. *et al.* Two-Dimensional Materials in Biosensing and Healthcare: From In Vitro Diagnostics to Optogenetics and Beyond. *ACS Nano*, **13**, 9781–9810 (2019).
25. Turtos, R. M. *et al.* On the use of the scintillating nanoplatelets as time taggers for high-energy gamma detection, NPJ 2D Mater. *Appl*, **3**, 37 (2019).
26. Thirimanne, H. M. *et al.* High sensitivity organic inorganic hybrid X-ray detectors with direct transduction and broadband response. *Nat. Commun*, **9**, 2926 (2018).

27. Kim, S., Lee, J. & Kang, J. Sensitivity Improvement of Quantum Dot-Blended Hybrid Detector for X-ray Imaging, Coatings 2020, 10, 222.
28. Seon, H., Ban, D. & Kang, J. Improvement of the sensitivit of organic polymer-based photodetector fabricated with p-type conjugated polymers for indirec X-ray detection. *J. Instrum*, **13**, C11009 (2018).
29. Kim, B., Lee, J. & Kang, J. Improving the sensitivity of indirect-type organic X-ray detector by blending with CdSe quantum dots. *J. Instrum*, **12**, C01009 (2017).
30. Liu, H., Lee, J. & Kang, J. Characteristics of a Hybrid Detector Combined with a Perovskite Active Layer for Indirect X-ray Detection. *Sensors*, **20**, 6872 (2020).
31. Kunneman, L. T. *et al.* Nature and Decay Pathways of Photoexcited States in CdSe and CdSe/CdS Nanoplatelets. *Nano Lett*, **14**, 7039–7048 (2014).
32. Feigl, C. A., Barnard, A. S. & Russo, S. P. Size- and shape-dependent phase transformations in wurtzite ZnS nanostructures. *Phys. Chem. Chem. Phys*, **14**, 9871–9879 (2012).
33. Scott, R. *et al.* Directed emission of CdSe nanoplatelets originating from strongly anisotropic 2D electronic structure. *Nat. Nanotechnol*, **12**, 1155–1160 (2017).
34. Jahandar, M. *et al.* High-Performance CH3NH3PbI3-Inverted Planar Perovskite Solar Cells with Fill Factor Over 83% via Excess Organic/Inorganic Halide, ACS Appl. *Mater. Interfaces*, **9**, 35871–35879 (2017).
35. Jovanovic, S., Spreitzer, M., Tramsek, M., Trontelj, Z. & Suvorov, D. Effect of Oleic Acid Concentration on the Physicochemical Propteries of Cobalt Ferrite Nanoparticles. *J. Phys. Chem. C*, **118**, 13844–13856 (2014).
36. Choi, S. *et al.* Partially pyridine-functionalized quantum dots for effcient red, green, and blue light-emitting diodes. *J. Mater. Chem. C*, **7**, 3429–3435 (2019).
37. dos Santos, J. A. L. *et al.* L. 3-Mercaptopropionic, 4-Mercaptobenzoic, and Oleic Acid-Capped CdSe Quantum Dots: Interparticle Distance, Anchoring Groups, and Surface Passivation, J. Nanomater 2019, 2019, 2796746.
38. Lokteva, I. *et al.* Surface Treatment of CdSe Nanoparticles for Application in Hybrid Solar Cells: The Effect of Multiple Ligand Exchange with Pyridine. *J. Phys. Chem. C*, **114**, 12784–12791 (2010).
39. Kwan, C. P. *et al.* Space-charge limited conduction in epitaxial chromia films grown on elemental and oxide-based metallic substrates. *AIP Adv*, **9**, 055018 (2019).
40. Haneef, H. F., Zeidell, A. M. & Jurchescu, O. D. Charge carrier traps in organic semiconductors: a review on the underlying physics and impact on electronic devices. *J. Mater. Chem. C*, **8**, 759–787 (2020).
41. Sareni, B., Krrahenbuhl, L., Brosseau, C. & Beroual, A. Effective dielectric constant of random composite materials. *J. Appl. Phys*, **81**, 2375 (1997).

Figures

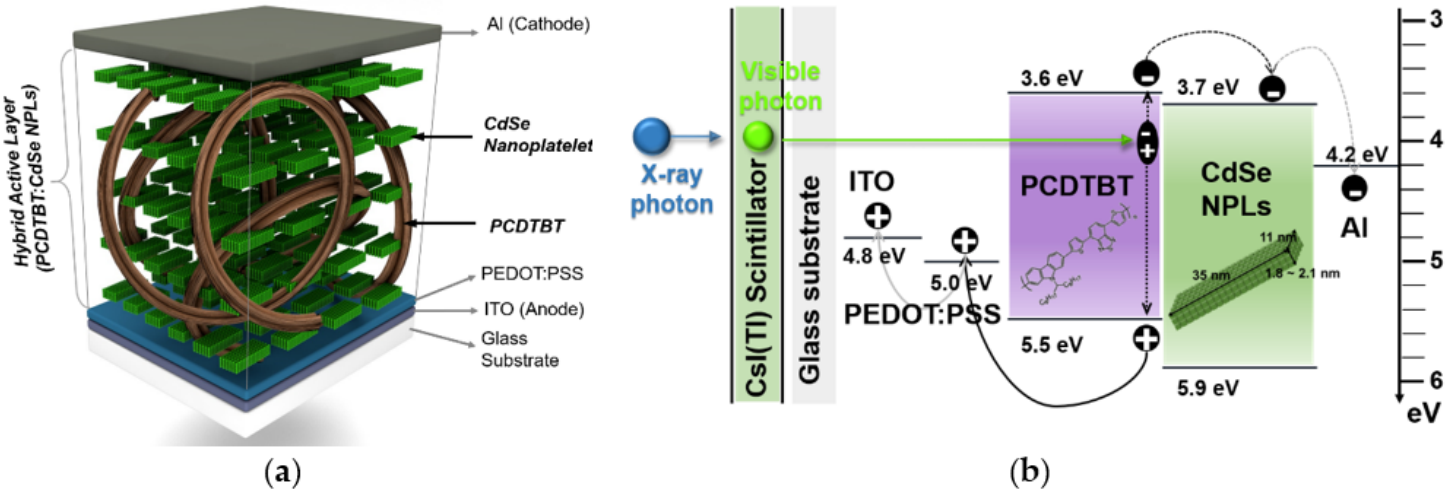

Figure 1

(a) The structure of the detector with PCDTBT:CdSe NPLs hybrid active layer and (b) the energy band diagram of the propsed detector.

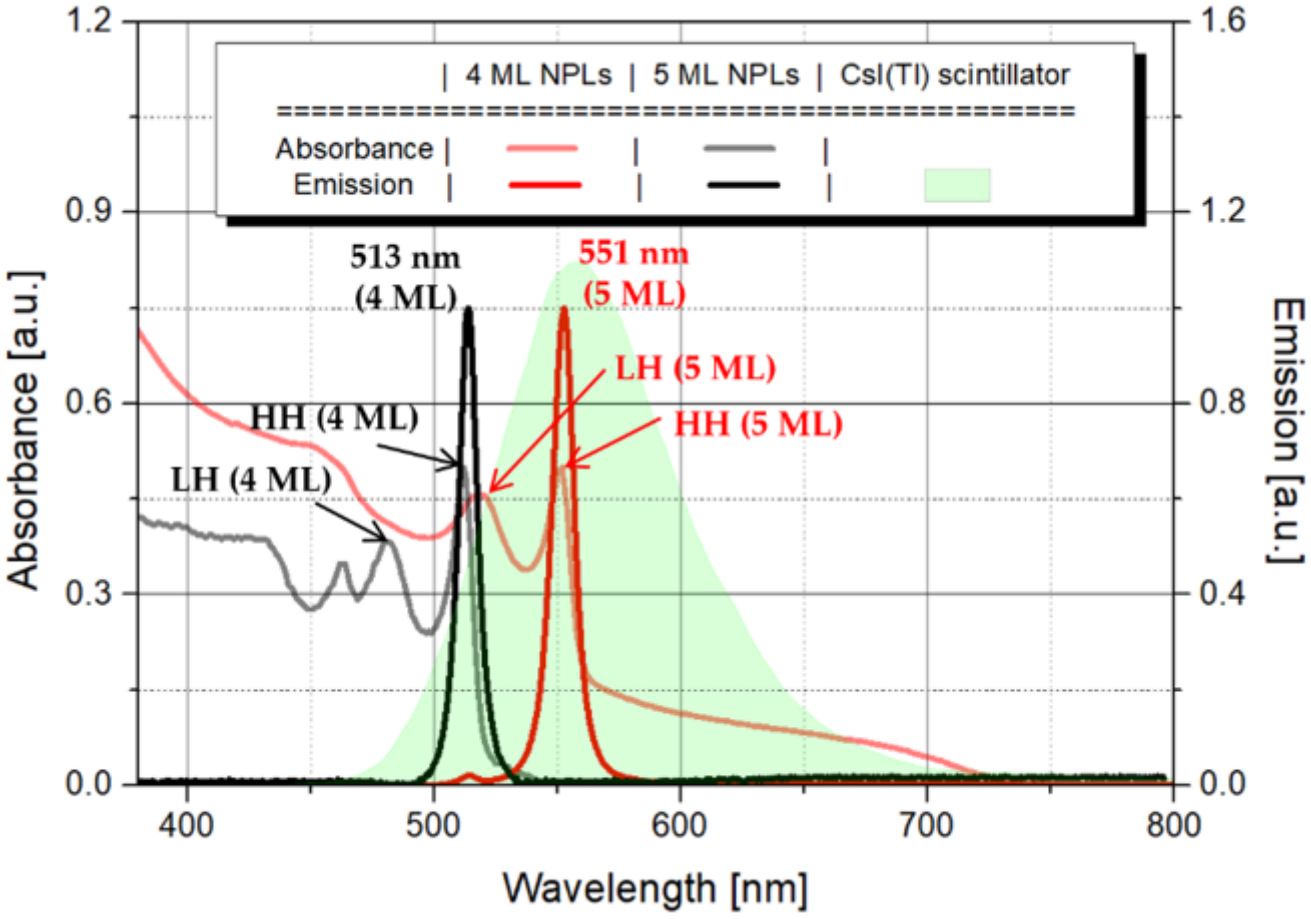

Figure 2

The absorption and emission spectrum of synthesized CdSe NPLs with either 4 and 5 monolayers thick and (b) CsI (Tl) scintillator emission spectrum with have 560 nm peak.

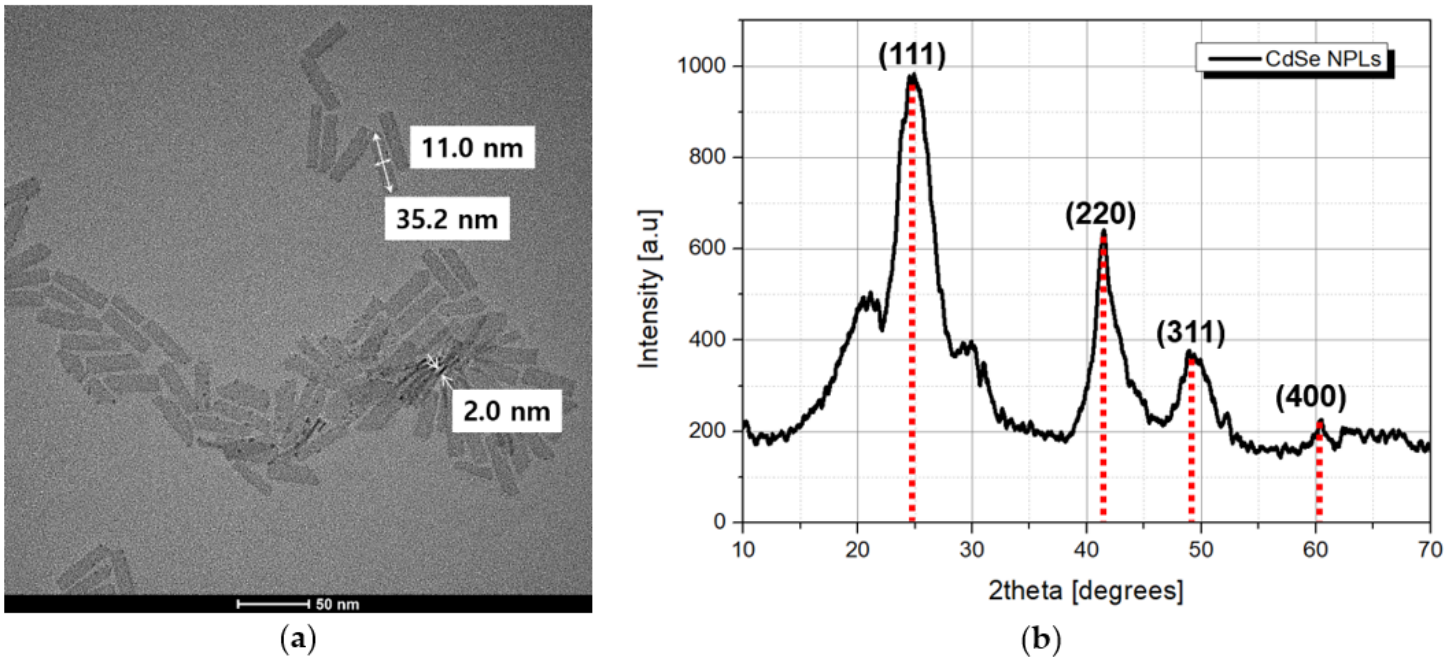

Figure 3

(a) The TEM image and (b) XRD pattern of synthesized 5 MLs thick CdSe NPLs.

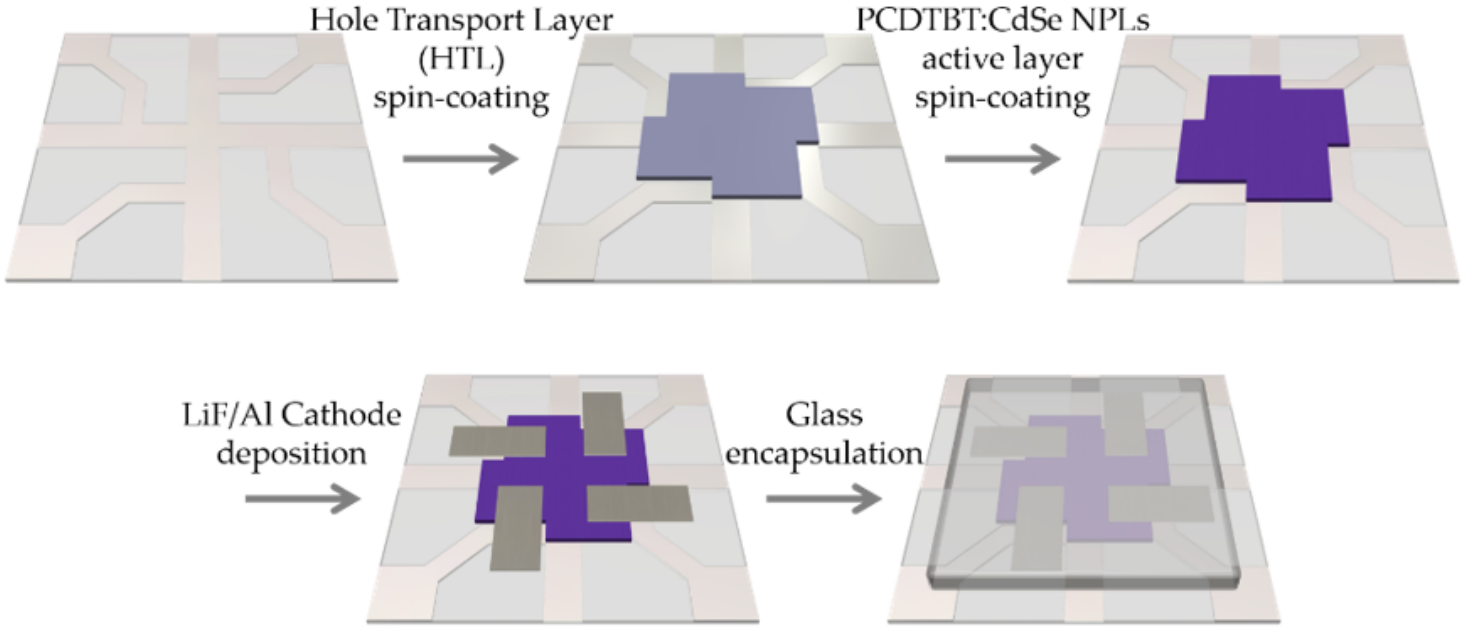

Figure 4

The fabrication process of the detector with PCDTBT:CdSe NPLs hybrid active layer.

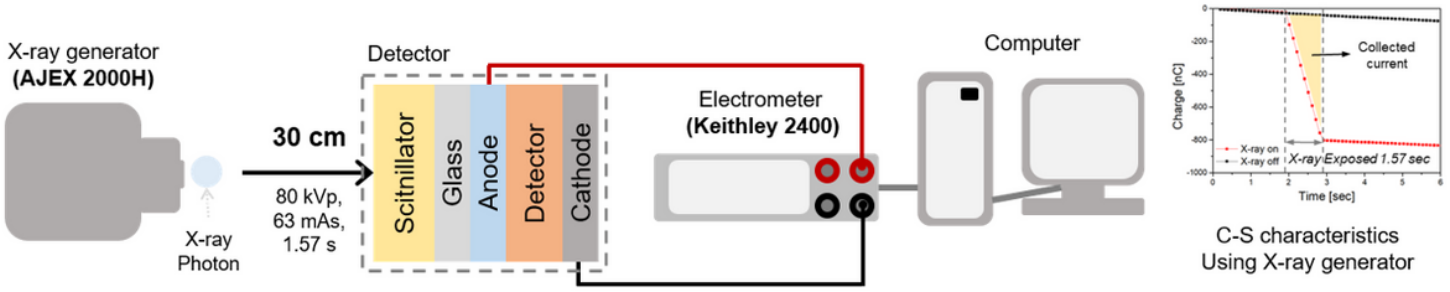

Figure 5

Schematics diagram of experimental set-up for measuring the X-ray parameters (CCD, DCD, and sensitivity).

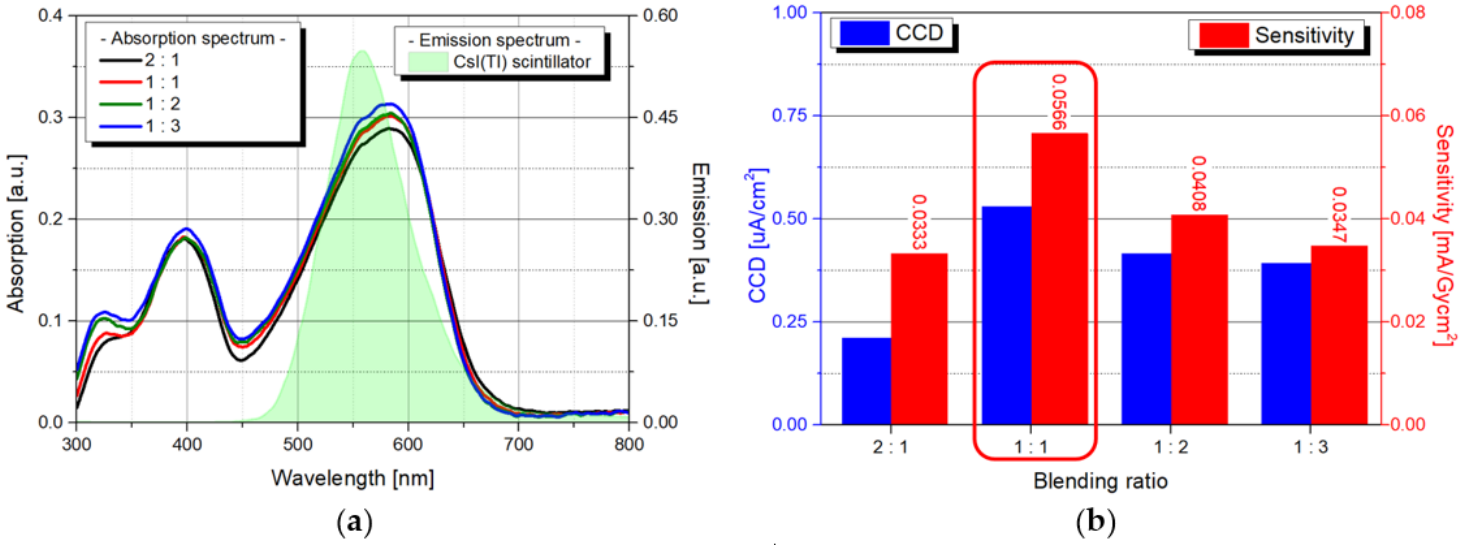

Figure 6

(a) The absorption spectrum of the film state PCDTBT:CdSe NPL hybrid active layer and the CsI (Tl) scintillator according to blending ratio, and (b) X-ray detector parameters such as CCD and sensitivity.

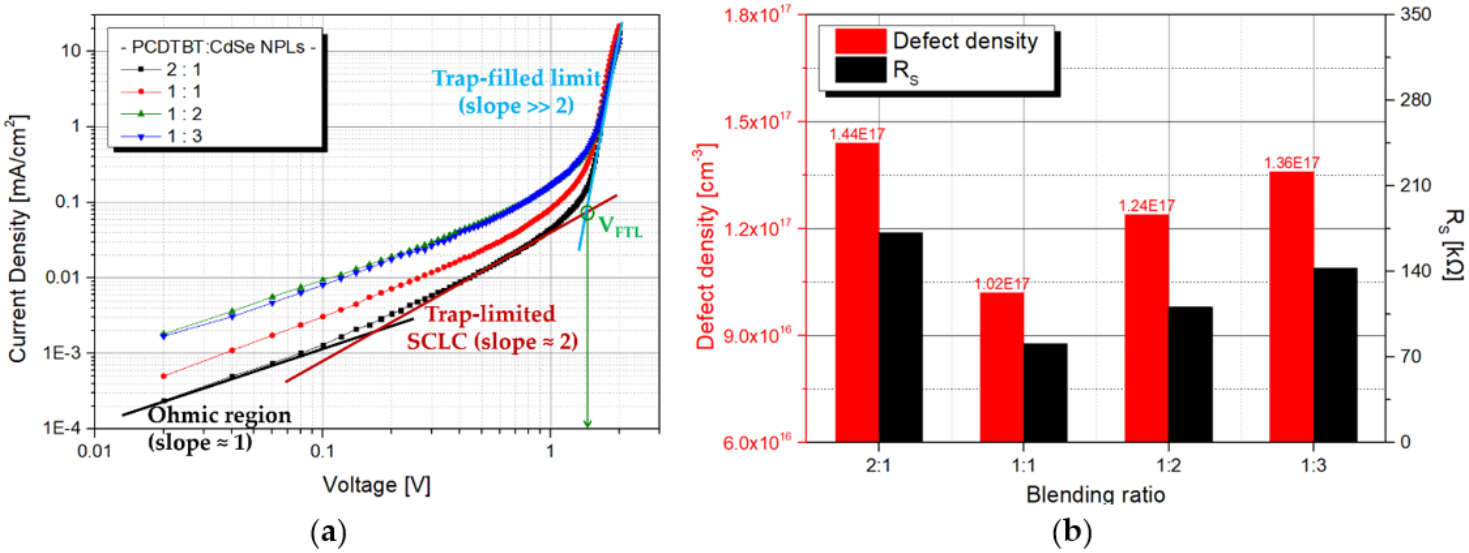

Figure 7

(a) The J-V curve of detector with PCDTBT:CdSe NPLs hybrid active layer for extract trap density under dark condition and (b) compare with defect density and RS according to PCDTBT:CdSe NPL blending ratio.

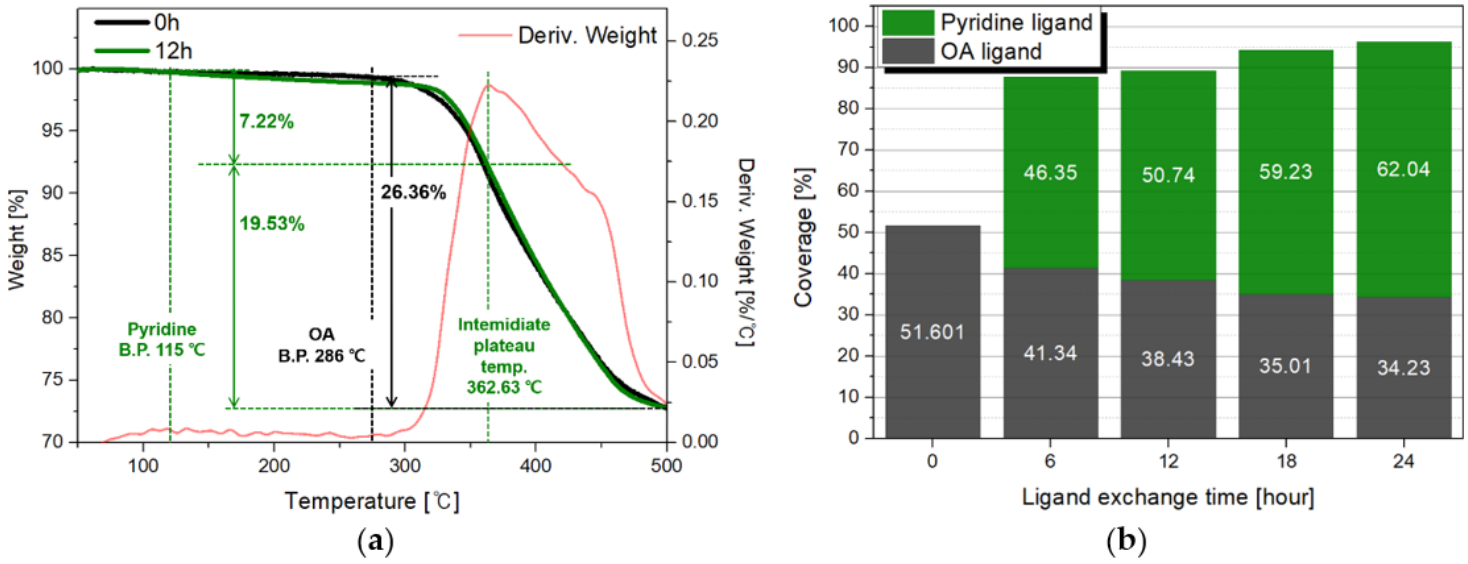

Figure 8

(a) The TGA graph of 0 and 12-hour pyridine ligand exchange time and (b) the cover proportion of OA and pyridine ligand on CdSe NPLs surface according to pyridine exchange time (0 to 24 hour).

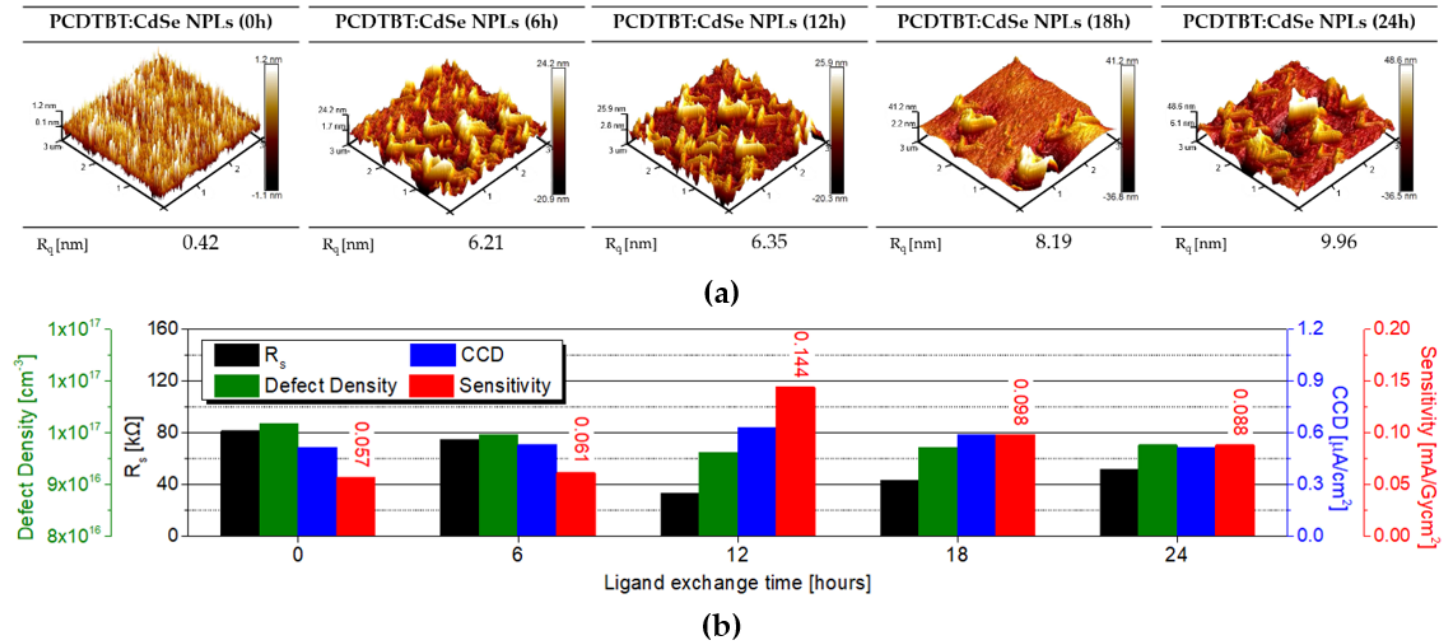

Figure 9

(a) The AFM image and Rq of PCDTBT:CdSe NPL film state and (b) the evaluate parameters such as the RS, defect density, CCD, and sensitivity of detector with PCDTBT:CdSe NPLs active layer according to

pyridine ligand exchange time.

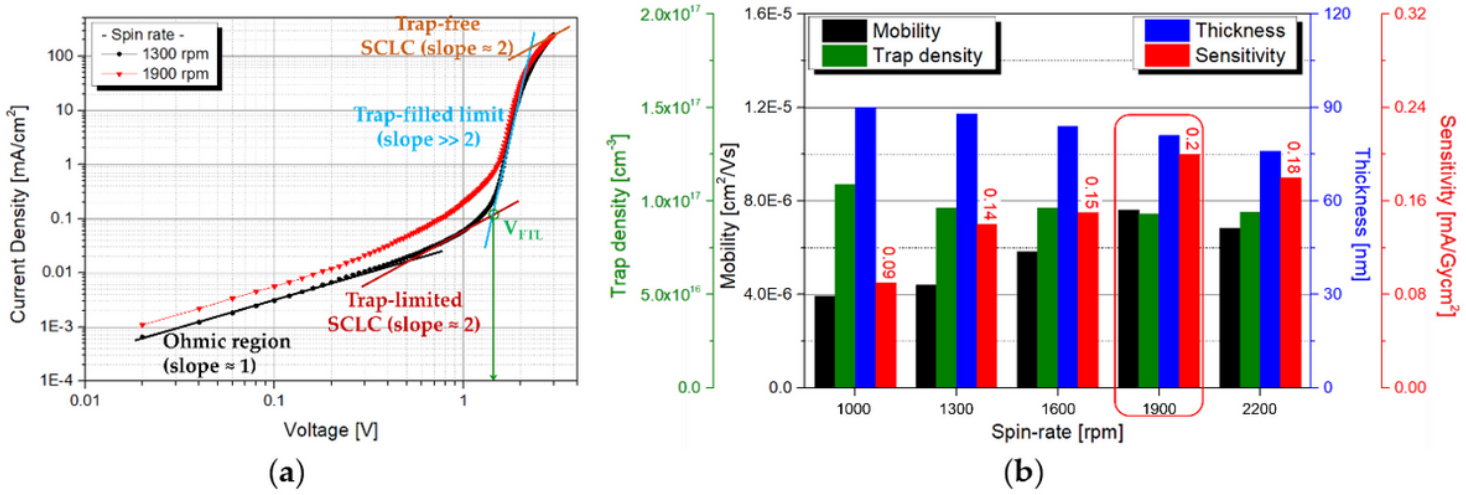

Figure 10

(a) J-V curve of PCDTBT:CdSe NPL detector for extract defect density and mobility under dark condition with spin rate of 1300 and 1900 rpm, and (b) the mobility, defect density, thickness and sensitivity according to the spin rate conditions.

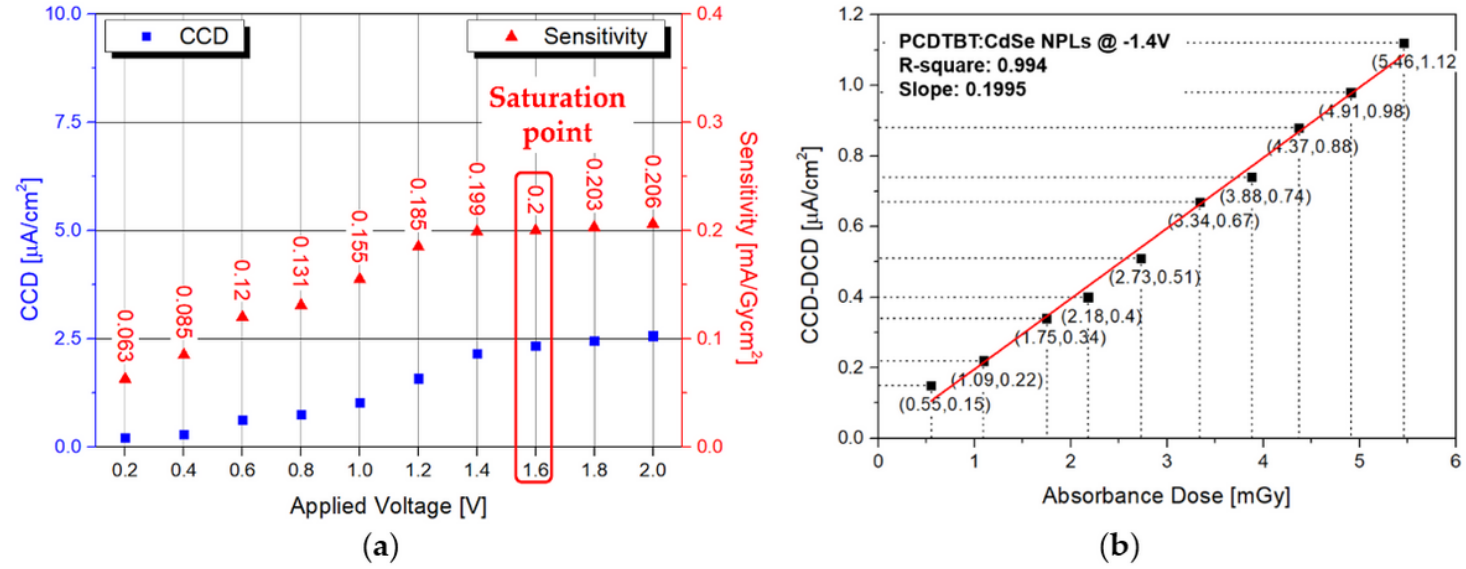

Figure 11

(a) The linearity of sensitivity with applied voltage on PCDTBT:CdSe NPLs hybrid detector and (b) CCD-DCD value of the detector with PCDTBT:CdSe NPLs depending on the absorbed dose.

Supplementary Files

This is a list of supplementary files associated with this preprint. Click to download.

- supplymentary.docx